Available online at www.sciencedirect.com
ScienceDirect
Journal of the European Ceramic Society 27 (2007) 143–150
www.elsevier.com/locate/jeurceramsoc

Creep behaviour of alumina/YAG nanocomposites obtained by a colloidal processing route

R. Torrecillas [a,*], M. Schehl [a], L.A. Díaz [a], J.L. Menéndez [a], J.S. Moya [b]

[a] *INCAR-CSIC, C/Francisco Pintado Fe 26, La Corredoria, 33011 Oviedo, Spain*
[b] *ICMM-CSIC, Campus UAM, Cantoblanco, 28049 Madrid, Spain*

Received 10 September 2005; received in revised form 3 April 2006; accepted 29 April 2006
Available online 27 June 2006

Abstract

The high temperature creep behaviour (1200–1400 °C and 30–250 MPa) of high-purity alumina (A) and an alumina/YAG nanocomposite (AY) prepared by using a colloidal processing route has been studied. Creep parameters were correlated with microstructural features in order to determine the dominant creep mechanisms in both materials.

It was found that the creep rate value of AY was 1 order of magnitude lower than the one of undoped alumina A. The creep mechanism for AY was found to be lattice diffusion (Nabarro–Herring) compared to a combination of grain boundary (Coble) and lattice diffusion for A. When the slow crack growth region of both materials was compared, a significant improvement was observed, i.e. the slow crack growth region of alumina shifted to nearly 2.5 times the stresses applied for AY at the temperatures of 1200, 1300 and 1400 °C.

Keywords: Powders-solid state reaction; Powders-chemical preparation; Nanocomposites; Creep; Al_2O_3; Al_2O_3/YAG

1. Introduction

Due to a good balance of properties (cost, sintering temperature, σ_f, K_{IC} and creep rate) alumina is at present, the most common ceramic material used for industrial applications.

The effect of dopants on the microstructural features and on the creep behaviour of alumina sintered compacts has constituted an active subject of research during the last 30 years.

The first attempts to dope alumina with metal cations were made by Hollenberg and Gordon,[1] using trivalent ions such as Fe^{3+} and Cr^{3+}. These researchers came to the conclusion that these ions only have a small influence on the creep rate of alumina. Dopant ions such as Fe^{2+}, Ni^{2+} and Ti^{4+} have generally been found to increase the creep rate of alumina.[1,2] Recently the role of yttrium-doped alumina has been the subject of several studies[3,4] (Table 1). From these results it was made clear that doping ultra-high-purity alumina with yttrium has a beneficial effect on high temperature deformation, as the creep rate of ultra-high-purity alumina can be lowered by at least 2 orders of magnitude. In these previous works the alumina was doped only with small quantities of large ions just below and slightly above the solubility limit. Then, only a small fraction, if any, of second phase was obtained (YAG). In a very recent paper Satapathy and Chokshi[5] report that alumina–5 vol.%YAG micrometer sized composite deform by a Coble grain boundary diffusion process.

The present work is focused on the impact of the presence of YAG nanoparticles at alumina grain boundaries on the creep operating mechanisms of alumina. A study of the high temperature slow crack growth region (SCG) given by pairs of critical stress and the corresponding critical strain rate at different temperatures was accomplished for mullite by Torrecillas et al.[6] A similar study for alumina and alumina/YAG nanocomposites is also proposed in the present investigation. This study would surely contribute to understand the complexity of the creep behaviour of this kind of composites.

2. Experimental procedure

2.1. Materials

A commercial high-purity α-alumina (Al_2O_3) powder (HPA-0.5, Condea, Hamburg, Germany) with $d_{50} = 0.46$ μm, a specific

* Corresponding author.
E-mail address: rtorre@incar.csic.es (R. Torrecillas).

0955-2219/$ – see front matter © 2006 Elsevier Ltd. All rights reserved.
doi:10.1016/j.jeurceramsoc.2006.04.177

Table 1
Influence of dopants on the creep rate of alumina ($\dot{\varepsilon}_A$)

Dopant (ppm)	Temperature (°C)	$\dot{\varepsilon}_{A+D}/\dot{\varepsilon}_A$	Reference
Y_2O_3 (1000)	1200	$\sim 10^{-2}$	5
Y_2O_3 (1000)	1250	$\sim 10^{-2}$	6
La_2O_3 (1000)	1250	$\sim 10^{-2}$	6
Lu_2O_3 (1753)	1250	2×10^{-2}	8,9
La_2O_3 (1437)	1250	5×10^{-3}	8,9
Y_2O_3 (996)	1250	5×10^{-3}	8,9

surface area of 9.9 m^2/g and 99.99% purity was used as starting material. The chemical analysis of this high-purity alumina powder is shown in Table 2. The alumina powder was sieved under 45 μm, cold isostatically pressed (CIP) at 200 MPa and finally sintered in air at 1600 °C for 2 h. The alumina sample was called A. The alumina crystals surface modification was achieved by colloidal processing following the powder-alkoxide route.[7] Then the alumina powder was dispersed in anhydrous 99.97% ethanol and by the drop wise addition of yttrium methoxyethoxide (ABCR, Germany) to the dispersion, the yttrium methoxyethoxide molecules were fixed to the alumina surface. The slurry was first dried under magnetic stirring at 70 °C and subsequently in air at 120 °C for 24 h in order to eliminate the rest of the alcohol. The dried powder was subsequently crushed to remove agglomerates resulting from the drying process. The powder was thermally treated at 850 °C for 2 h in order to remove organic residuals and to precipitate the Y_2O_3 nanoparticles on the alumina grains surface (Fig. 1) and subsequently attrition-milled with alumina balls for 30 min. After drying, the powder was sieved under 45 μm. The powder thus obtained was cold isostatically pressed (CIP) at 200 MPa and sintered in air at 1600 °C for 2 h. The sample was called AY.

2.2. Characterisation techniques

Creep tests were carried out in air in a four-point-bending fixture at temperatures ranging from 1200 to 1400 °C under stresses ranging from 30 to 250 MPa using an Instron 8562 testing machine. The heating rate of the furnace was 300 °C/h in order to avoid significant thermal gradients and thermal instabilities. In order to ensure dimensional stability for all parts of the testing machine, the holding time at the test temperature was 1 h. At the corresponding temperature a constant load P was immediately applied and the specimen deflection (on the tensile face) at the centre of the sample and the load applied were recorded as a function of time.

Table 2
Chemical analysis of α-Al_2O_3 powder (Condea, HPA-0.5)

	Trace impurities (ppm)
Na	19
Si	25
Fe	14
Ca	4
Mg	4
Ga	<4
Cr	3
Ni	<1
Ti	8
Mn	1
Cu	<1
Mo	<4
Li	<1
Zn	1
Zr	4

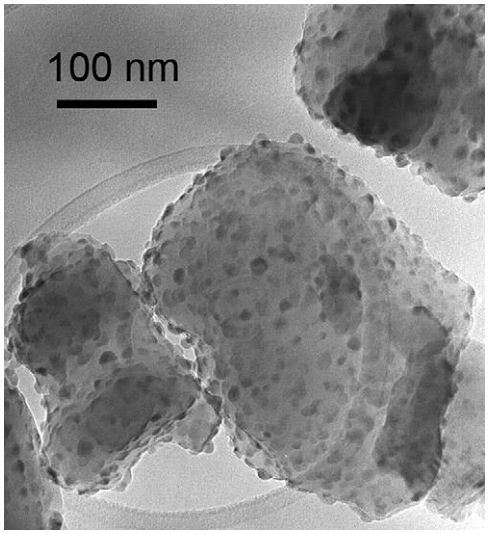

Fig. 1. TEM image of starting alumina–nY_2O_3 powders.

The specimens were parallelepipeds with the following dimensions: b (sample width) 4 mm, w (sample height) 3 mm, l (sample length) 35 mm (4 mm × 3 mm × 35 mm). The tensile face of all the specimens was polished with diamond paste down to 3 μm and the edges were chamfered (about 45°) in order to avoid the influence of microcracks on creep behaviour.

A four-point-bending fixture of alumina with an outer span of 28 mm and an inner span of 14 mm was used and the flexural stress on the tensile face of the specimen was calculated by the following expression:

$$\sigma = \frac{3P(L - L')}{2bw^2} \quad (1)$$

where P is the applied load, L the outer span, L' the inner span, b the sample width and w is the sample height.

Hollenberg et al.[8] showed that the creep strain ε can be calculated from the deflection y at the centre of the specimen, if there is no major cracking in the specimen and the deflection y is small compared to the inner span L':

$$\varepsilon = K(n)y \quad (2)$$

$K(n)$ being calculated as

$$K(n) = \frac{2w(n+2)}{(L - L')[L + L'(n+1)]} \quad (3)$$

The constant $K(n)$, in addition to its dependence on n, is also a function of the spans L and L'. Hollenberg et al.[8] have shown that for (L/L') values close to 2, $K(n)$ is almost insensitive to the n value. So, expression (2) can be used and ε calculated with

an approximate value for n. In the case of a too high divergence between the determined n and the initially supposed n, calculations for ε must be made again.

For microstructural observations by scanning electron microscopy (SEM), the surfaces of the sintered specimens were polished and thermally etched at 1400 °C/1 h to reveal grain morphologies. Grain sizes on the polished surfaces were measured by using image analysis software (Leica QWin Standard V 2.3, Leica, Germany).

3. Results and discussion

3.1. Microstructure

Fig. 2(a) and (b) shows the microstructure of the non-deformed samples A and AY, respectively. Alumina (A) shows a dense and homogenous microstructure with a mean grain size of 5.9 μm. All alumina grains are nearly equiaxed. Sample AY has a dispersion of second phase particles, located at alumina grain boundaries and triple points. These second phase particles at alumina grain boundaries are yttrium aluminium garnet (YAG). All of these YAG particles are located at grain boundaries or triple points. Only very few intragranular YAG nanoparticles were found and almost all alumina triple points are occupied by second phase nanoparticles. The distribution of the YAG particles throughout the alumina matrix was found to be very homogeneous with a mean particle size of 200 nm for YAG and 3.6 μm for alumina grains, respectively. This is a direct consequence of the highly homogeneous distribution of the Y_2O_3 in the starting alumina powder (Fig. 1) which was obtained by using the mentioned colloidal route.[7] This result contrast with the heterogeneous distribution and bimodal microstructures obtained in previous works.[5]

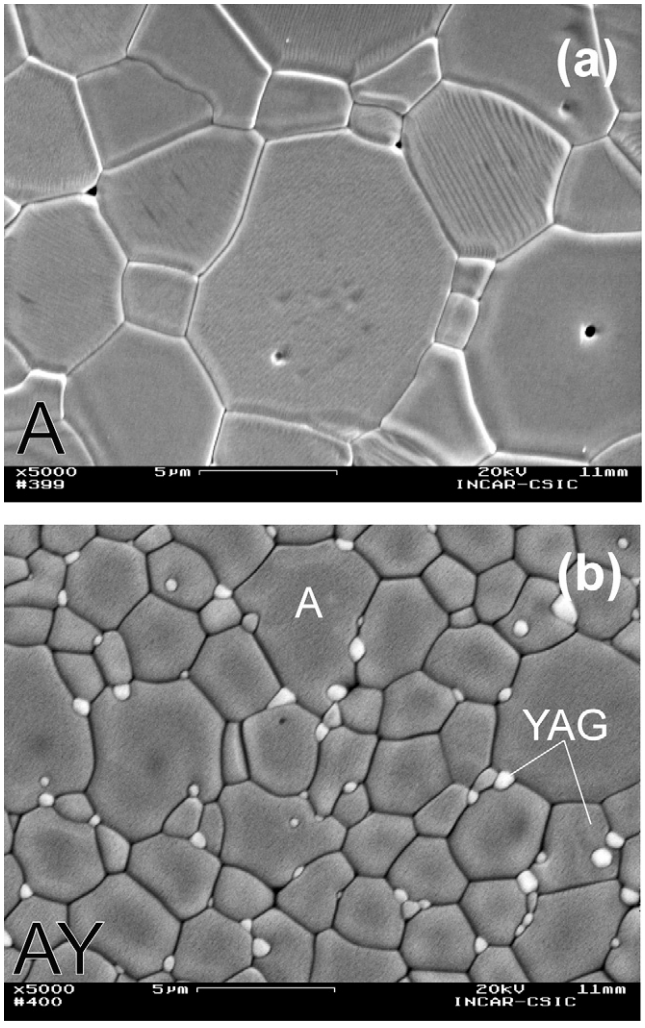

Fig. 2. SEM micrograph of (a) A and (b) AY.

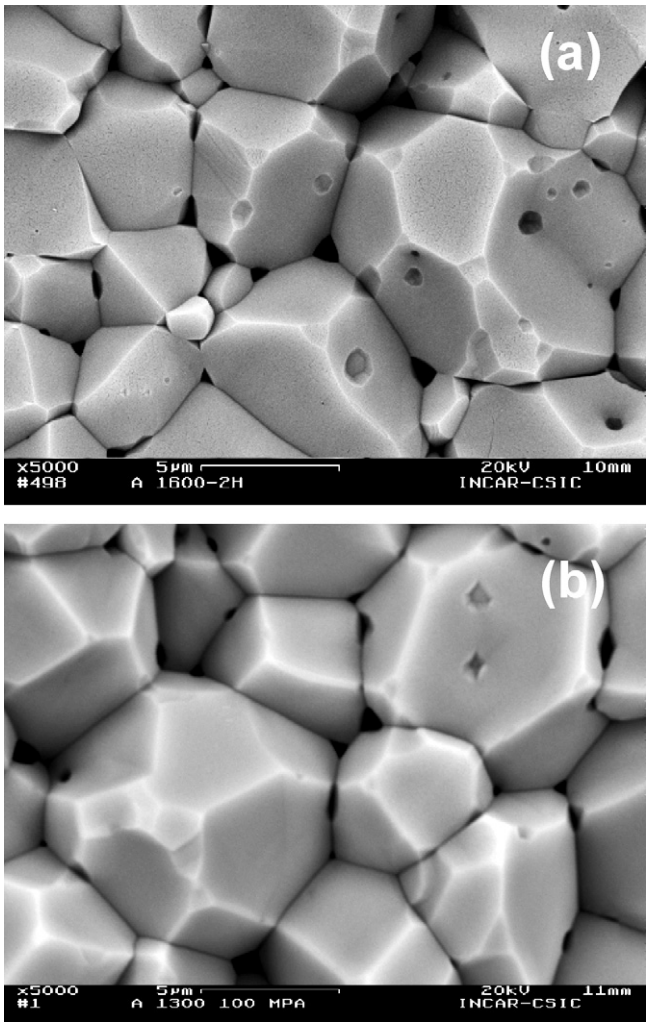

Fig. 3. Fracture surfaces of A (a) before and (b) after creep measurements.

Fig. 3(a) and (b) and Fig. 4(a) and (b) show the fracture surfaces at room temperature and after creep measurements in the case of slow crack growth for A and AY, respectively. It is evident that no significant grain growth occurred during creep deformation.

3.2. Creep parameters and slow crack growth

The creep behaviour of A and AY at 1300 °C is shown in Fig. 5(a) and (b) in a strain versus time plot. For A the applied stresses range from 30 to 100 MPa, while for the AY

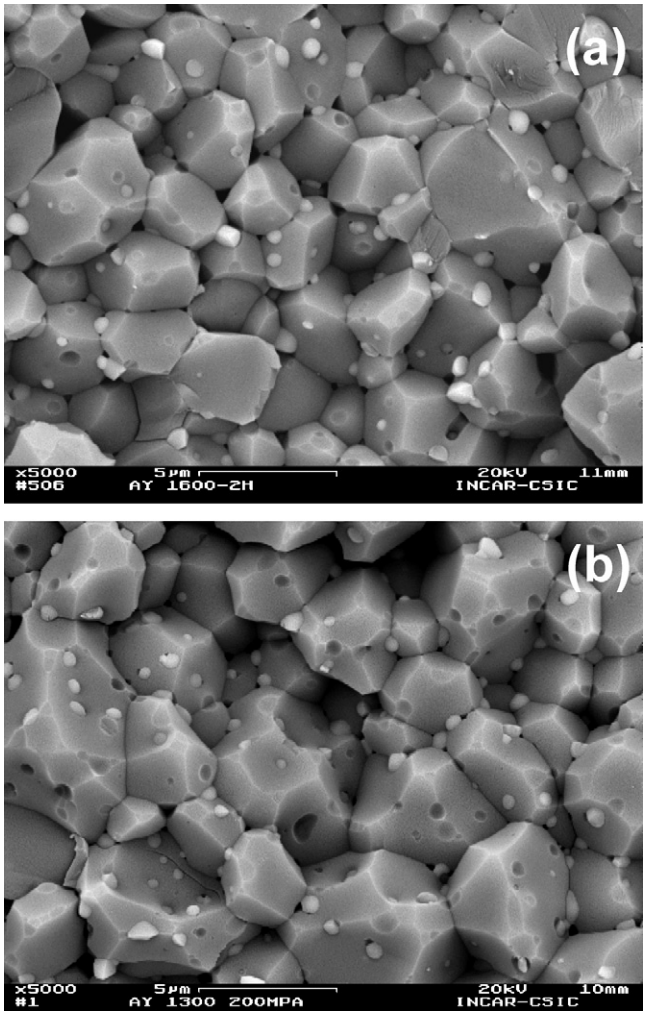

Fig. 4. Fracture surfaces of AY (a) before and (b) after creep measurements.

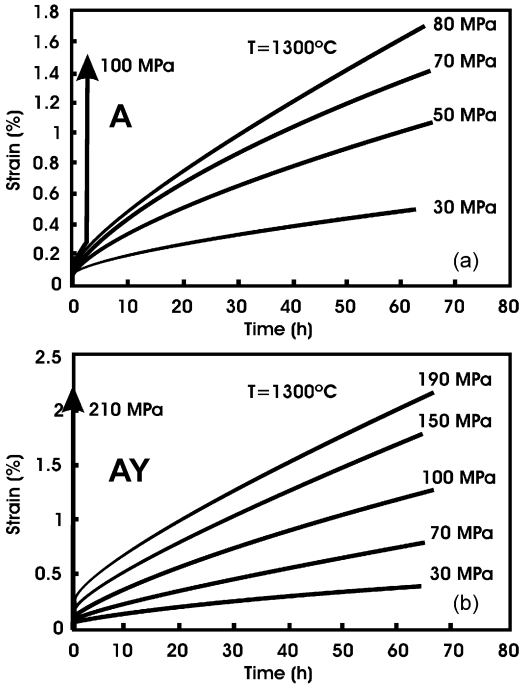

Fig. 5. Creep curves of (a) A and (b) AY at 1300 °C.

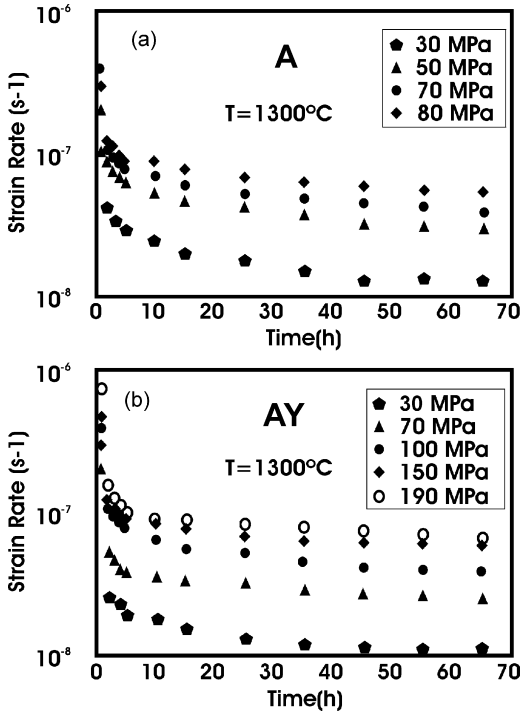

Fig. 6. Strain rate evolution vs. time for (a) A and (b) AY at 1300 °C.

nanocomposite they range from 30 to 210 MPa. All creep curves show only the primary creep and steady-state creep region. No tertiary creep region was observed, even in the case of fracture surfaces of broken specimens. Both materials A and AY reached the steady-state at 1300 °C for all applied stresses as can be observed in Fig. 6(a) and (b) in a strain rate versus time plot. Considering the time interval 0–65 h, no specimen fracture was observed for A up to an applied stress of 80 MPa, whereas for AY an applied stress of 190 MPa was possible without there occurring any fracture in the sample. At 1300 °C fracture occurred for alumina at an applied stress of 100 MPa, while 210 MPa were necessary in the case of AY composites in order to observe fracture of the specimen as a result of slow crack growth. Fracture of sample A took place approximately after 4 h, whereas fracture of AY occurred after 5 min. This difference in fracture behaviour for A and AY at 1300 °C was also observed at 1200 and 1400 °C. In the slow crack growth region A deforms somewhere between 2 and 4 h before fracture, while the fracture for AY occurs after short time intervals (0–5 min).

It should be noted that with a relatively small quantity of YAG nanoparticles at grain boundaries and triple points, the slow crack growth region of alumina shifts from 80 MPa for A to 190 MPa for AY at 1300 °C, nearly 2.5 times the applied stress.

The steady-state creep rate $\dot{\varepsilon}$ is expressed by the following equation:

$$\dot{\varepsilon} = A\frac{\sigma^n}{d^p}\exp\left(-\frac{Q}{RT}\right) \tag{4}$$

where A is a material constant, σ the applied stress, n the stress exponent, d the grain size, p the grain size exponent, Q the

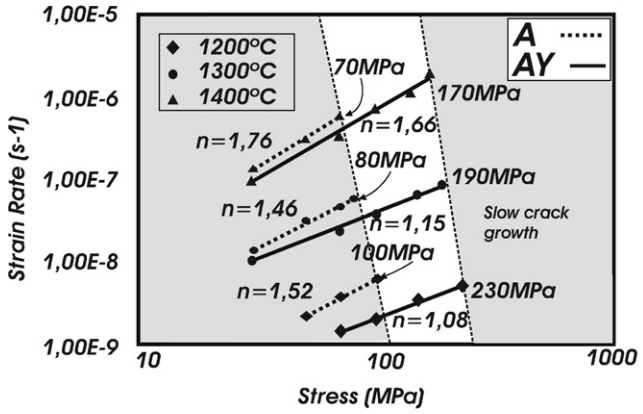

Fig. 7. Steady-state creep rate vs. applied stress for A and AY.

activation energy for creep, R the gas constant and T is the absolute temperature.

A complete creep behaviour characterisation for A and AY was performed in the temperature range of 1200–1400 °C with different applied stresses in order to determine the stress exponents n for a given temperature and the activation energies Q for a given stress.

Fig. 7 shows the steady-state creep rate as a function of the applied stress in a log–log plot for A and AY, respectively. The applied stresses were 30–120 MPa for A and 30–250 MPa for AY in the 1200–1400 °C temperature range. The stress exponents n for A and AY were determined for the constant temperatures 1200, 1300 and 1400 °C. The stress exponents n for A at 1200 °C ($n = 1.52$) and 1300 °C ($n = 1.46$) were nearly the same. At 1400 °C the stress exponent rises to $n = 1.76$. Sample AY has a stress exponent of 1.08 at 1200 °C and 1.15 at 1300 °C. At 1400 °C the stress exponent rises to 1.66. Both materials show only small differences for n at 1200 and 1300 °C, which may be attributed to experimental scatter. At 1400 °C the values of n for both materials rise.

Fig. 8(a) and (b) shows the relationship of the steady-state creep rate $\dot{\varepsilon}$ and the reciprocal of the absolute temperature $1/T$ on a $\log \dot{\varepsilon} - 1/T$ plot for A and AY, respectively. The stresses used for the determination of the activation energies Q were 50 and 70 MPa for A, while for AY stresses of 70 and 100 MPa were applied. The temperature range was 1200–1400 °C for both materials. For A with an applied stress of 50 MPa the activation energy was 517 kJ/mol, whereas for an applied stress of 70 MPa the calculated activation energy was 527 kJ/mol. AY has an activation energy Q of 554 kJ/mol for an applied stress of 70 MPa and 595 kJ/mol for an applied stress of 100 MPa.

In Fig. 7 two regions can be clearly discerned: a region where no specimen fracture occurs in the time interval of 0–65 h and another region where specimen fracture occurs. The latter is called the slow crack growth region. Both regions can be clearly separated by a straight line for both materials, A and AY. This line is given by pairs of critical stress and the corresponding critical strain rate for the temperatures 1200, 1300, 1400 °C, respectively. For A this slow crack growth region can be defined by the following values: 1200 °C, 100 MPa; 1300 °C, 80 MPa; 1400 °C,

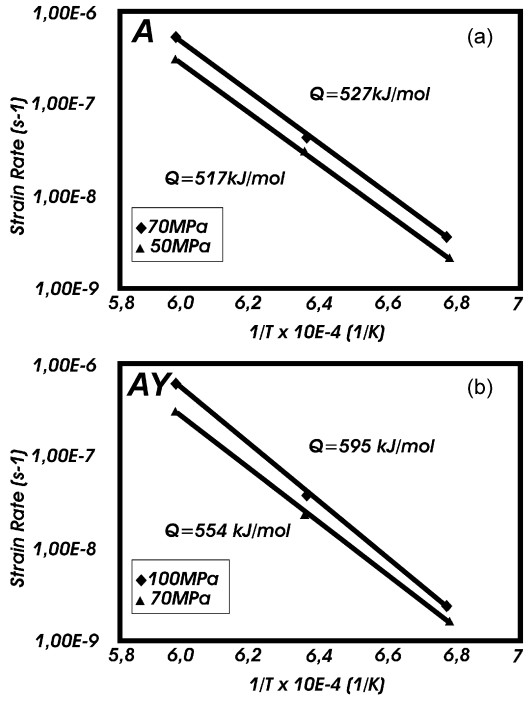

Fig. 8. Steady-state creep rate vs. reciprocal of the absolute temperature for (a) A and (b) AY.

70 MPa and their corresponding strain rates. Between these three points a straight line can be drawn in the log strain rate–log applied stress diagram, clearly marking the slow crack growth region of A. For AY the slow crack growth region can be defined by the following values: 1200 °C, 230 MPa; 1300 °C, 190 MPa; 1400 °C, 170 MPa and their corresponding strain rates. For this material a straight line can also be drawn between these three points, clearly separating the slow crack growth region for AY. Fig. 7 shows that the slow crack growth region has been shifted to nearly 2.5 times the stresses applied in the temperature range of 1200–1400 °C for AY material.

Li et al.[9] determined stress exponent values close to $n = 2$ for the doped and undoped materials, i.e. materials with and without small quantities of second phase particles. They pointed out the possibility of interface reaction in the creep process. Yoshida et al.[10] reported stress exponents of about 2 and they justified this value in terms of either interface reaction-controlled diffusional creep[11] or grain boundary sliding.[12,13,14] In their subsequent study they confirmed this assumption.[10] Corman[15] has studied the creep behaviour of single crystalline YAG and demonstrated that YAG is much more creep resistant than single crystal alumina (sapphire). For polycrystalline YAG, Parthasarathy et al.[16] reported a stress exponent of 1.1 at 1500 °C and 1.24 at 1610 °C. They attributed the deformation to a Nabarro–Herring creep mechanism. French et al.[17] obtained a stress exponent of 2.6 for polycrystalline YAG, admitting that this was somewhat higher than that previously reported.[16]

In this study the stress exponent for A is around 1.5 at 1200 and 1300 °C. This value is comparable to stress exponents determined for alumina by other researchers.[18] For AY the stress exponent determined is nearly 1 at 1200 and 1300 °C. Thus it

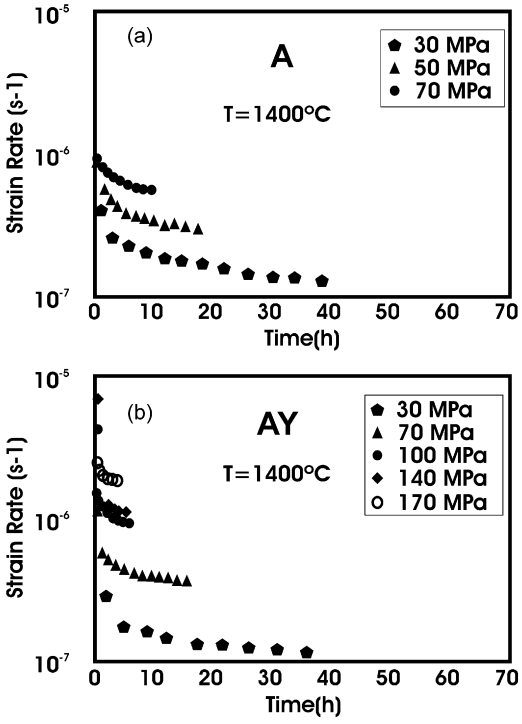

Fig. 9. Strain rate evolution vs. time for (a) A and (b) AY at 1400 °C

may be concluded that the small quantity of YAG nanoparticles is controlling the creep behaviour of AY. As a consequence, lattice diffusion (Nabarro–Herring) must be the controlling mechanism in this composite. At 1400 °C the values of n for both materials, A and AY, rise. These values can be overestimated. This overestimation becomes clear in Fig. 9(a) and (b), where the strain rate is represented as a function of time. At 1400 °C and with high applied stresses the curves are still in the primary creep region, signifying that the steady-state has not yet been reached. Therefore the calculated strain rates cannot be considered as steady-state creep rates.

The activation energies calculated for A were 517 and 527 kJ/mol for an applied stress of 50 and 70 MPa, respectively (Fig. 8(a) and (b)). The activation energy for Al^{3+} grain boundary diffusion is 420 kJ/mol, whereas for Al^{3+} lattice diffusion the activation energy is 578 kJ/mol.[18–20] A comparison of these values with the measured values suggests that both Al^{3+} grain boundary diffusion and Al^{3+} lattice diffusion are active in the measured temperature range of 1200–1400 °C. Cannon and Coble[18] obtained a similar result for Mg-doped Al_2O_3 with grain sizes in the range of 1–15 μm, suggesting cation boundary control for the fine-grained material and cation lattice control for the larger-grained materials, but with the contribution of boundary diffusion, especially at lower temperatures. Taking into account the fact that the measured grain size of A was 5.9 μm and the temperature range was 1200–1400 °C, the results obtained in the present study agree with the ones obtained in the mentioned works. Thus a combination of grain boundary diffusion controlled creep and lattice diffusion controlled creep must be the dominant creep mechanism for A. The measured stress exponent of 1.5 at 1200 and 1300 °C for A confirms this supposition. The calculated activation energies for AY were 554 and 595 kJ/mol for an applied stress of 70 and 100 MPa, respectively (Fig. 8(a) and (b)). These values were lower than the activation energies measured for Y-doped Al_2O_3 in the literature. French et al.[17] obtained 698 kJ/mol for the activation energy of a 1000 ppm yttrium-doped Al_2O_3 with an applied stress of 75 MPa in the 1125–1350 °C temperature range. In a subsequent study[21] these researchers calculated 685 kJ/mol for the same material with an applied stress of 50 MPa in the temperature range of 1200–1350 °C. Yoshida et al.[22] obtained 830 kJ/mol for Al_2O_3 doped with 0.045 mol% Y_2O_3 for an applied stress of 100 MPa in the 1250–1350 °C temperature range. The creep of polycrystalline YAG was examined by Parthasarathy et al.[16] and French et al.[17] calculated an activation energy of 586 kJ/mol for an applied stress of 75 Pa in the 1250–1350 °C temperature range, while Parthasarathy et al.[16] found 549 kJ/mol for an applied stress of 45 MPa and 579 kJ/mol for an applied stress of 300 MPa. A comparison of these values with the results obtained for AY indicates that the controlling mechanism is lattice diffusion (Nabarro–Herring). The measured stress exponent of nearly 1 at 1200 and 1300 °C confirms this assumption.

The differences observed in the creep behaviour of the AY nanocomposite and A can be explained as follows. A combination of grain boundary diffusion controlled creep and lattice-diffusion controlled creep is assumed to be the dominant creep mechanism of alumina. When YAG particles are formed at alumina grain boundaries during sintering, sliding of alumina grains should only be possible if YAG nanoparticles are deformed. The high activation energy required to deform these YAG nanoparticles as well as the strong influence that nanosizes have on all thermally activated mechanisms (assuming there are no defects present in the nanoparticles, like dislocations, vacancies, etc.) are very well known. As a consequence, the activation energy associated with the grain boundary diffusion of Al_3^+ will rise to values close to those corresponding to the lattice diffusion of YAG nanoparticles. The activation energy of the lattice diffusion of Al_3^+ is very similar to the activation energy of the lattice diffusion of polycrystalline YAG and thus the deformation mechanism operating in this composite will be lattice diffusion. The measured stress exponents of 1.08 at 1200 °C and 1.15 at 1300 °C and the activation energies of 554 kJ/mol determined for an applied stress of 70 MPa and 595 kJ/mol for an applied stress of 100 MPa clearly point to this deformation mechanism.

In Fig. 8(a) and (b) it can be seen that the strain rate of AY is lower over the whole temperature range than that corresponding to A, which signifies that AY has more or less half the strain rate of A for an applied stress of 70 MPa. In order to compare these results, the differences in grain sizes of both materials have to be considered. For lattice-diffusion controlled creep the grain size exponent p is 2 and for grain boundary diffusion controlled creep the grain size exponent is 3.[23–25] The creep rates of sample AY were normalised with the grain size exponent 2, assuming that the dominant creep mechanism for AY is lattice diffusion (Nabarro–Herring). Thus, taking into account the differences in grain sizes for A and AY, a normalised strain rate for AY $\dot{\varepsilon}_{n\mathrm{AY}}$

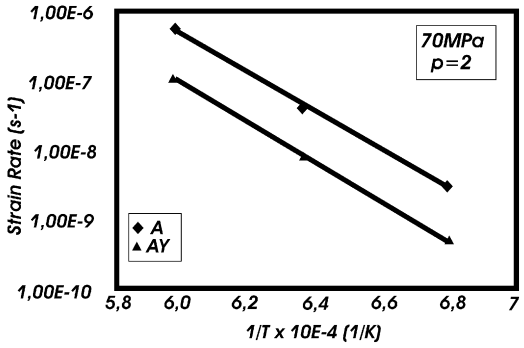

Fig. 10. Normalised creep rates with $p = 2$ for (a) A and (b) AY.

can be defined as

$$\dot{\varepsilon}_{n\mathrm{AY}} = \left(\frac{1}{d_{\mathrm{A}}/d_{\mathrm{AY}}}\right)^{p} \dot{\varepsilon}_{\mathrm{AY}} \tag{5}$$

where $\dot{\varepsilon}_{\mathrm{AY}}$ is the measured creep rate for AY, d_{A} is the mean grain size of alumina and d_{AY} is the mean grain size of AY. The results of the normalisation for a grain size exponent of 2 are shown in Fig. 10. It can be observed that the strain rate of A is reduced by approximately one order of magnitude.

In summary it can be stated that the creep behaviour of AY is controlled by the small volume fraction of YAG nanoparticles located at the grain boundaries of alumina. The calculated stress exponent and activation energy lead to the conclusion that the dominant creep mechanism for AY is lattice diffusion (Nabarro–Herring).

The effect of the presence of a second phase at the matrix grain boundaries on the activation energy values was also studied by Wang and Raj[26] in the case of alumina–zirconia ceramics suggesting that the bonding at the interface influences diffusion transport.

The slow crack growth region for both materials is limited by maximum stress and the corresponding strain rate for the temperatures 1200, 1300 and 1400 °C. The creep region can be characterised by the uniform values of the stress exponent, activation energy and low strain rates, while the slow crack growth region (SCG) is characterised by slow crack growth and ultimately catastrophic failure in a brittle manner. To avoid the risk of catastrophic failure of A and AY at high temperatures, the range of stresses and temperatures at which deformation occurs via accommodated creep and not by creep damage or slow crack growth has to be determined. For A this slow crack growth region can be defined by the following values: 1200 °C, 100 MPa; 1300 °C, 80 MPa; 1400 °C, 70 MPa, whereas for AY the following values were determined: 1200 °C, 230 MPa; 1300 °C, 190 MPa; 1400 °C, 170 MPa. This signifies that the slow crack growth region has been shifted by nearly 2.5 times the stresses applied over the temperature range of 1200–1400 °C.

4. Conclusions

The colloidal processing route used in this study leads to a very homogeneous microstructure with YAG nanoparticles located at nearly all triple points and alumina grain boundaries.

The presence of the YAG nanoparticles changes the deformation mechanisms and thus the creep behaviour is completely different to that of pure alumina. The sliding of alumina grains is blocked by the presence of the YAG nanoparticles. Due to the high activation energy required to deform YAG nanoparticles, the activation energy associated with the grain boundary diffusion of Al^{3+} rises to values close to those of the lattice diffusion of YAG nanoparticles. It can be deduced, therefore, that the deformation mechanism operating in this composite is lattice diffusion.

Because of this, a significant improvement (nearly 2.5 times the stresses applied in the 1200–1400 °C temperature range) of the threshold at which slow crack growth at high temperatures appears is achieved in alumina/YAG nanocomposite.

Acknowledgements

The authors would like to acknowledge the help of the EU for the financial support received under the GROWTH2000 project reference BIOKER G5RD-CT-2001-00483, IP NANOKER NMP3-CT-2005-515784 and the support of the Spanish Ministry of Education and Science project reference MAT2003-04199-C02-01.

References

1. Hollenberg, G. W. and Gordon, R. S., Effect of oxygen partial-pressure on creep of polycrystalline Al_2O_3 doped with Cr, Fe, or Ti. *J. Am. Ceram. Soc.*, 1973, **56**, 140–147.
2. Lessing, P. A. and Gordon, R. S., Creep of polycrystalline alumina, pure and doped with transition-metal impurities. *J. Mater. Sci.*, 1977, **12**, 2291–2302.
3. Korinek, S. L. and Dupau, F., Grain-boundary behavior in superplastic Mg-doped alumina with yttria codoping. *Acta Metall. Mater.*, 1994, **42**, 293–302.
4. Carry, C. and Mocellin, A., Structural superplasticity in single-phase crystalline ceramics. *Ceram. Int.*, 1987, **13**, 89–98.
5. Satapathy, L. N. and Chokshi, A. H., Microstructural development and creep deformation in an alumina–5% yttrium aluminum garnet composite. *J. Am. Ceram. Soc.*, 2005, **88**, 2848–2854.
6. Torrecillas, R., Calderón, J. M., Moya, J. S., Reece, M. J., Davies, C. K. L., Olagnon, C. and Fantozzi, G., Suitability of mullite for high temperature applications. *J. Eur. Ceram. Soc.*, 1999, **19**, 2519–2527.
7. Schehl, M., Díaz, L. A. and Torrecillas, R., Alumina nanocomposites from powder-alkoxide mixtures. *Acta Mater.*, 2002, **50**, 1125–1139.
8. Hollenberg, G. W., Terwillinger, G. R. and Gordon, R. S., Calculation of stresses and strains in 4-point bending creep tests. *J. Am. Ceram. Soc.*, 1971, **54**, 196–199.
9. Li, Y. Z., Wang, C., Chan, H. M., Rickman, J. M., Harmer, M. P., Chabala, J. M., Gavrilov, K. L. and Levi-Scotti, R., Codoping of alumina to enhance creep resistance. *J. Am. Ceram. Soc.*, 1999, **82**, 1497–1504.
10. Yoshida, H., Ikuhara, Y. and Sakuma, T., A critical factor to determine the high-temperature creep resistance in cation-doped polycrystalline Al_2O_3. *Key Eng. Mater.*, 2000, **171–174**, 809–816.
11. Burton, B., Interface reaction controlled diffusional creep-consideration of grain-boundary dislocation climb sources. *Mater. Sci. Eng.*, 1972, **10**, 9–14.
12. Mukherjee, A. K., Rate controlling mechanism in superplasticity. *Mater. Sci. Eng.*, 1971, **8**, 83–89.
13. Gifkins, R. C., Grain-boundary sliding and its accommodation during creep and superplasticity. *Metall. Trans. A*, 1976, **7A**, 1225–1232.
14. Arieli, A. and Mukherjee, A. K., A model for the rate-controlling mechanism in superplasticity. *Mater. Sci. Eng.*, 1980, **45**, 61–70.
15. Corman, G. S., Creep of yttrium–aluminium–garnet single-crystals. *J. Mater. Sci. Lett.*, 1993, **12**, 379–382.

16. Parthasarathy, T. A., Mah, T. I. and Keller, K., Creep mechanism of polycrystalline yttrium–aluminium–garnet. *J. Am. Ceram. Soc.*, 1992, **75**, 1756–1759.
17. French, J. D., Zhao, J., Harmer, M. P., Chan, H. M. and Miller, G. A., Creep of duplex microstructures. *J. Am. Ceram. Soc.*, 1994, **77**, 2857–2865.
18. Cannon, R. M. and Coble, R. L., In *Deformation of Ceramic Materials*, ed. R. C. Bradt and R. E. Tressler. Plenum Press, New York, 1975. pp. 61–100.
19. Cannon, R. M., Rhodes, W. H. and Heuer, A. H., Plastic-deformation of fine-grained alumina (Al_2O_3). 1. Interface-controlled diffusional creep. *J. Am. Ceram. Soc.*, 1980, **63**, 46–53.
20. Heuer, A. H., Tighe, N. J. and Cannon, R. M., Plastic-deformation of fine-grained alumina (Al_2O_3). 2. Basal slip and non-accommodated grain-boundary sliding. *J. Am. Ceram. Soc.*, 1980, **63**, 53–58.
21. Cho, J. H., Harmer, M. P., Chan, H. M., Rickman, J. M. and Thompson, A. M., Effect of yttrium and lanthanum on the tensile creep behavior of aluminum oxide. *J. Am. Ceram. Soc.*, 1997, **80**, 1013–1017.
22. Yoshida, H., Ikuhara, Y. and Sakuma, T., High-temperature creep resistance in rare-earth-doped, fine-grained Al_2O_3. *J. Mater. Res.*, 1998, **13**, 2597–2601.
23. Nabarro, F. R. N., Steady-state diffusional creep. *Phil. Mag.*, 1967, **16**, 231–237.
24. Herring, C., Diffusional viscosity of a polycrystalline solid. *J. Appl. Phys.*, 1950, **21**, 437–445.
25. Coble, R. L., A model for boundary diffusion controlled creep in polycrystalline materials. *J. Appl. Phys.*, 1963, **34**, 1679–1682.
26. Wang, J. D. and Raj, R., Activation-energy for the sintering of 2-phase alumina zirconia ceramics. *J. Am. Ceram. Soc.*, 1991, **74**, 1959–1963.